Free Radical Biology and Medicine 65 (2013) 828–837

Contents lists available at ScienceDirect

Free Radical Biology and Medicine

journal homepage: www.elsevier.com/locate/freeradbiomed

Original Contribution

In vivo detection of free radicals in mouse septic encephalopathy using molecular MRI and immuno-spin trapping

Rheal A. Towner [a,*], Philippe Garteiser [a,1], Fernando Bozza [b], Nataliya Smith [a], Debra Saunders [a], Joana C.P. d'Avila [b], Flora Magno [b], Marcus F. Oliveira [c], Marilyn Ehrenshaft [d], Florea Lupu [e], Robert Silasi-Mansat [e], Dario C. Ramirez [f], Sandra E. Gomez-Mejiba [f], Ronald P. Mason [d], Hugo C. Castro Faria-Neto [g]

[a] Advanced Magnetic Resonance Center, Oklahoma Medical Research Foundation, Oklahoma City, OK 73104, USA
[b] Instituto de Pesquisa Clinica Evandro Chagas, Instituto Oswaldo Cruz, Fiocruz, Rio de Janeiro, RJ, Brazil
[c] Laboratório de Bioquímica de Resposta ao Estresse, Programa de Biologia Molecular e Biotecnologia, Instituto de Bioquímica Médica, Universidade Federal do Rio de Janeiro, Cidade Universitária, Rio de Janeiro, RJ, Brazil
[d] Laboratory of Pharmacology and Chemistry, National Institute of Environmental Health Sciences, Research Triangle Park, NC 27709, USA
[e] Cardiovascular Biology, Oklahoma Medical Research Foundation, Oklahoma City, OK 73104, USA
[f] Laboratory of Experimental Medicine & Therapeutics, Instituto Multidisciplinario de Investigaciones Biologicas–San Luis, CONICET, National University of San Luis, San Luis 5700, Argentina
[g] Laboratório de Imunofarmacologia, Instituto Oswaldo Cruz, Fiocruz, Rio de Janeiro, RJ, Brazil

ARTICLE INFO

Article history:
Received 20 June 2013
Received in revised form
16 August 2013
Accepted 17 August 2013
Available online 23 August 2013

Keywords:
Immuno-spin trapping
Free radicals
Molecular MRI
Sepsis
Cecal ligation and puncture
Mice
in vivo
DMPO
Fluorescence microscopy
4-Hydroxynonenal
3-Nitrotyrosine

ABSTRACT

Free radicals are known to play a major role in sepsis. Combined immuno-spin trapping and molecular magnetic resonance imaging (MRI) was used to detect in vivo and in situ levels of free radicals in murine septic encephalopathy after cecal ligation and puncture (CLP). DMPO (5,5-dimethyl pyrroline *N*-oxide) was injected over 6 h after CLP, before administration of an anti-DMPO probe (anti-DMPO antibody bound to albumin–gadolinium–diethylene triamine pentaacetic acid–biotin MRI targeting contrast agent). In vitro assessment of the anti-DMPO probe in oxidatively stressed mouse astrocytes significantly decreased T_1 relaxation ($p < 0.0001$) compared to controls. MRI detected the presence of anti-DMPO adducts via a substantial decrease in % T_1 change within the hippocampus, striatum, occipital, and medial cortex brain regions ($p < 0.01$ for all) in septic animals compared to shams, which was sustained for over 60 min ($p < 0.05$ for all). Fluorescently labeled streptavidin was used to target the anti-DMPO probe biotin, which was elevated in septic brain, liver, and lungs compared to sham. Ex vivo DMPO adducts (qualitative) and oxidative products, including 4-hydroxynonenal and 3-nitrotyrosine (quantitative, $p < 0.05$ for both), were elevated in septic brains compared to shams. This is the first study that has reported on the detection of in vivo and in situ levels of free radicals in murine septic encephalopathy.

Oxidative stress-generated reactive oxygen (and nitrogen) species (ROS/RNS)[2] play a pathogenic role in many diseases, either as modulators of signal transduction or as causative agents of tissue injury. Understanding the extent and timing of free radical-triggered events in an in vivo environment is of importance to our understanding of these major determinants involved in disease evolution and prognosis. With the combined use of molecular magnetic resonance imaging (mMRI) and immuno-spin trapping (IST) technologies, it is possible for the first time to monitor radicals in vivo and in situ in a mouse model for septic encephalopathy.

Numerous studies indicate that oxidative stress, a result of an imbalance in the levels of ROS and antioxidative defense systems, plays a crucial role in sepsis. Sepsis is associated with the increased generation of ROS [1–5], which leads to multiple organ dysfunctions [6], including encephalopathy and its cognitive consequences [7]. ROS/RNS may directly oxidize nucleic acids, proteins, carbohydrates, and lipids, causing intracellular and intercellular perturbations in homeostasis [8]. As a consequence, high concentrations of lipid-derived electrophilic products readily react with proteins, DNA, and

Abbreviations: anti-DMPO probe, anti-DMPO-biotin-BSA-Gd-DTPA; BBB, blood–brain-barrier; BSA, bovine serum albumin; CLP, cecal ligation and puncture; DMPO, 5,5-dimethyl-1-pyrroline-*N*-oxide; Gd-DTPA, gadolinium diethylene triamine pentaacetic acid; HNE, 4-hydroxynonenal; IST, immuno-spin trapping; mMRI, molecular magnetic resonance imaging; 3-NT, 3-nitrotyrosine; OMRI, Overhauser-enhanced MRI; ROS/RNS, reactive oxygen/nitrogen species

* Corresponding author. Fax: +405 271 7254.
E-mail address: Rheal-Towner@omrf.org (R.A. Towner).
[1] *Current address:* Centre de Recherche Biomédicale Bichat-Beaujon, INSERM U773, Paris, France.

0891-5849/$ - see front matter © 2013 Elsevier Inc. All rights reserved.
http://dx.doi.org/10.1016/j.freeradbiomed.2013.08.172

phospholipids, generating intra- and intermolecular toxic covalent adducts that lead to the propagation and amplification of oxidative stress [8].

Free radicals generated as a result of oxidative stress processes can be tagged by 5,5-dimethyl-1-pyrroline *N*-oxide (DMPO) to form DMPO–radical adducts, which can be detected and measured by IST, a method that utilizes an antibody against DMPO adducts [9–12]. To better understand disease pathogenesis, it would be ideal if the formation of oxidation products could be assessed in vivo and in situ, allowing specific cause–consequence relationships to be identified from specific oxidative events. This approach would allow the correlation of the detection of real-time oxidative stress markers with specific longitudinal pathological conditions associated with a particular disease.

There are other imaging methods that have been used to detect radicals, including ESR (electron spin resonance), fluorescence imaging, and Overhauser-enhanced MRI (OMRI). OMRI potentially offers a method of detecting low concentrations of free radical species generated by specific biological processes; however, spatial resolution and general radical detection is limited by sensitivity requirements and only nonspecific probes have been validated [13]. ESR imaging is sensitive, but limited to the detection of an injected paramagnetic probe at the injection site and not the general detection of a broad range of radicals. Fluorescence imaging is restricted to excised tissues or isolated cells. Recently in vivo nitroxide-enhanced MRI, which shows some promise, was done in tumor (neuroblastoma or colon cancer)-bearing mice, in which the appearance or disappearance of the MRI signal indicated a change in the nitroxide (piperidine- or TEMPO-type derivatives) redox cycle, i.e., reduction to the hydroxylamine resulted in the loss of MRI contrast and oxidation resulted in the presence of MRI contrast [14].

In a novel approach, we have combined a Gd-DTPA-albumin-based contrast agent for signal detection with the specificity of antibodies (Abs) for DMPO radicals (anti-DMPO probe) with the desired morphological image resolution of mMRI to detect in vivo free radicals (see Fig. 1). The anti-DMPO probe was used in this study to assess free-radical formation in the brain, liver, and lung tissues in a mouse model of sepsis.

Materials and methods

Synthesis of DMPO-specific MRI contrast agents

To recognize the DMPO–protein/lipid radicals, a mouse monoclonal anti-DMPO antibody bound to a contrast agent was used. The macromolecular contrast material, biotin-BSA-Gd-DTPA, was prepared using a modification of the method of Dafni et al. [15]. The biotin moiety in the contrast material was added to allow histological localization. Biotin-BSA-Gd-DTPA was synthesized as described in Towner et al. [16,17]. A solution of biotin-BSA-Gd-DTPA was added directly to the solution of antibody (anti-DMPO, 200 μg/ml) for conjugation through a sulfo-NHS-EDC link between albumin and antibody according to the protocol of Hermanson [18]. The product was lyophilized and subsequently stored at 4 °C and reconstituted to the desired concentration for injections in phosphate-buffered saline (PBS). The final amount of the product, anti-DMPO-biotin-BSA-Gd-DTPA, that was injected into the mice was estimated to be 20 μg anti-DMPO Ab/injection and 10 mg biotin-BSA-Gd-DTPA/injection. The estimated molecular weight of the anti-DMPO-biotin-BSA-Gd-DTPA probe was estimated to be 232 kDa.

In vitro characterization of anti-DMPO probe

Vials were prepared containing water, primary mouse astrocytes alone, astrocytes with the anti-DMPO probe, astrocytes + DMPO + anti-DMPO probe, astrocytes with the oxidant hydrogen peroxide (H_2O_2) and DMPO, or astrocytes with H_2O_2 + DMPO + anti-DMPO probe ($n = 5$ for each group). Cells (mouse astrocytes, CC-3187, Lonza Walkersville, Walkersville, MD, USA) were grown to confluency in flasks in complete growth medium (ABM basal medium, Lonza Walkersville). Two to three hours before treatment, the growth medium was replaced with serum-free medium. DMPO (40 mM) was added to the appropriate vials, and after 15 min to reach equilibrium, H_2O_2 (50 μM) was added to the appropriate vials. In the samples that were treated with the anti-DMPO probe, the probe was added (2 μg, based on antibody

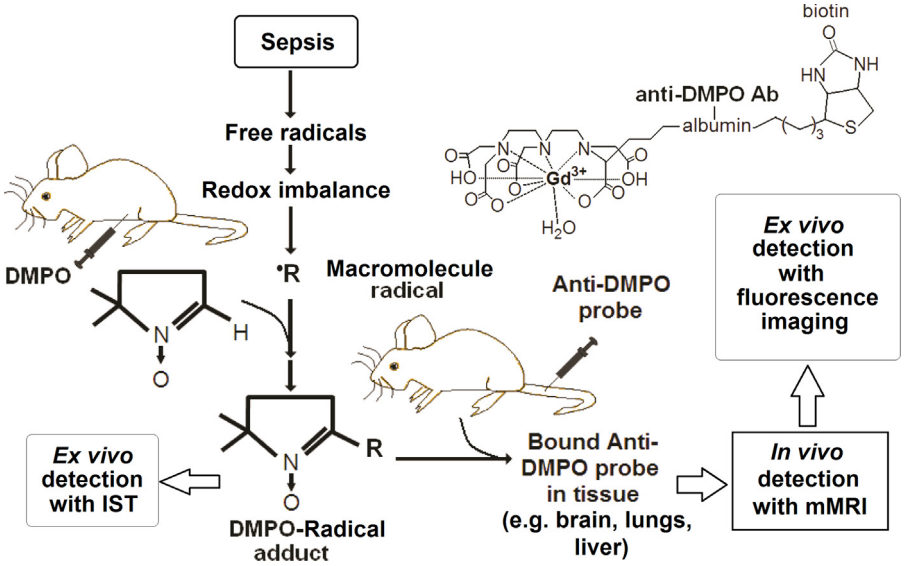

Fig. 1. Approach for combined in vivo mMRI and IST. Immuno-spin trapping of macromolecular radicals (•R) with anti-DMPO mMRI probe (anti-DMPO–albumin–Gd–DTPA–biotin mMRI probe). DMPO is injected ip to trap macromolecular radicals and generate DMPO–radical adducts that decay to DMPO nitrone adducts. Anti-DMPO is injected iv to target DMPO–radical nitrone adducts, which can be visualized by mMRI.

calculation), and the cells were incubated for 45 min. After incubation, the cells were collected, washed with PBS, and centrifuged (3000 rpm), and the cell pellet was resuspended in PBS (200 μl) for MR imaging. Any DMPO–radical adducts not bound to cells or free DMPO was washed away in the PBS and separated by centrifugation, and therefore only cell-bound DMPO–radical adducts were left in the cell fraction for assessment.

Animal experiments

All animal experiments were conducted in accordance with the National Institutes of Health animal use and welfare guidelines and with the authorization of the institutional animal ethics committee.

As a model for sepsis, CLP was used and performed as previously described by Gomes et al. [19]. Eight- to 10-week-old male C57BL/6 mice ($n = 6$; $n = 3$ CLP and $n = 3$ sham) were anesthetized with isoflurane (2–3%) under aseptic conditions. A laparotomy was performed with a 2-cm midline incision through the linea alba. The cecum was exposed and ligated with sterile 3-0 silk below the ileocecal junction. The cecum was punctured once with an 18-gauge needle and squeezed to empty its contents through the puncture. The cecum was returned to the peritoneal cavity, and the abdominal muscle and skin incisions were closed. After the surgery, 0.5 ml of sterile saline was administered subcutaneously to the animals. Mice in the sham operation control group were subjected to identical procedures, except that ligation and puncture of the cecum were omitted.

DMPO administration

DMPO (Alexis Biochemicals, Enzo Life Sciences, Farmingdale, NY, USA) was administered (25 μl in 100 μl saline, ip) every 1.5 h over a period of 6 h after CLP, before injection of the anti-DMPO probe.

Magnetic resonance techniques

For the in vitro study, signal intensities were obtained using fast low-angle shot (repetition time (TR) 125.3 ms, echo time (TE) 6.0 ms, flip angle 30°, 256 × 128 matrix, four signal averages per acquisition, 4.00 × 4.00-cm^2 field of view (FOV), 1-mm slice thickness). T_1 maps were obtained using a RARE (rapid acquisition with relaxation enhancement variable TR) sequence (TR 200, 400, 800, 1200, and 1600 ms; TE 15 ms; 256 × 256 matrix; two signal averages per acquisition; 4.00 × 4.00-cm^2 FOV; slice thickness 1.0 mm). Pixel-by-pixel relaxation maps were reconstructed from a series of T_1-weighted images using a nonlinear two-parameter fitting procedure.

MR experiments were carried out under general anesthesia (1–2% isoflurane, 0.8–1.0 L/min O_2). MR equipment that was used included a Bruker Biospec 7.0 Tesla/30-cm horizontal-bore imaging spectrometer. Anesthetized (2% isoflurane), restrained mice were placed in an MR-compatible cradle and inserted into an MR probe, and their brains were localized by MRI. Images were obtained using a Bruker S116 gradient coil (2.0 mT/m/A) and a 72-mm quadrature multirung RF coil. Mouse brains were imaged 6 h after CLP.

Multiple brain ^{1}H MR image slices were taken in the transverse plane using a spin echo multislice (TR 0.8 s, TE 23 ms, 128 × 128 matrix, four steps per acquisition, 3 × 4-cm^2 FOV, 1-mm slice thickness). Mouse brains were imaged at 0 (precontrast), 15, 30, 45, 60, and 75 min post-contrast agent injection to obtain kinetic data on targeted contrast agent distribution. Mice were injected intravenously with anti-DMPO antibody tagged with a biotin-Gd-DTPA-albumin-based contrast agent (200 μl/kg; 1 mg antibody/kg; 0.4 mmol Gd^{3+}/kg) [16,17]. T_1-weighted images were obtained using a variable TR spin-echo sequence. Pixel-by-pixel relaxation maps were reconstructed from a series of T_1-weighted images using a nonlinear two-parameter fitting procedure. The T_1 value of a specified region-of-interest (ROI) was computed from all the pixels in the ROI by the following equation [20] (processed by ParaVision 4.0, Bruker): $S(\mathrm{TR}) = S_0(1 - e^{-\mathrm{TR}/\mathrm{T1}})$, where TR is the repetition time (ms), S_0 is the signal intensity (integer machine units) at $\mathrm{TR} \gg T_1$ and $\mathrm{TE} = 0$, and T_1 is the constant of the longitudinal relaxation time (ms). Relative probe (contrast agent) concentrations, C (molar), were calculated for each of the selected ROIs (minimum of 10 ROIs obtained per region) using the following formula [20]: $C \propto (1/T_1(\mathrm{after}) - 1/T_1(\mathrm{before}))$, where $1/T_1$(after) is the T_1 rate taken at various time points after injection of probes, and $1/T_1$(before) is the T_1 rate taken before injection of probes.

Excised tissues

Cardiac perfusion with PBS was performed while the mice were under anesthesia (isoflurane), and then the heads were cut off using a guillotine. The skin and the muscle tissues were removed from the head. Then the bones on the top of the head were carefully removed, from the cerebellum to the olfactory bulb through the bregma and from one side of the head to the other side. The ear bones were carefully extracted from the brain; the optic chiasm and the olfactory bulb were excised to extract the brain. A transverse cut was then performed to get a sample for histology analysis in the brain tissue from septic animals. Liver and lung tissues were also excised and prepared for fluorescence microscopy.

Immunohistochemistry

Excised brain, liver. and lung tissues were cut and fixed in Z-fixative (zinc formalin: formaldehyde 10%, zinc sulfate heptahydrate 1%). The tissues were then rinsed with PBS and incubated with 15% sucrose before being embedded in optimal cutting temperature compound and frozen in liquid nitrogen.

Immunohistochemical staining of DMPO–radical nitrone adducts was done by incubating tissue sections (obtained 3 h after the last DMPO injection) with a mouse monoclonal anti-DMPO antibody (1:10) and a secondary antibody, a goat anti-mouse IgG conjugated to Texas red (1:100). In both cases, antibody dilutions were performed in 0.1% Tween 20 in PBS.

To target the Gd-based anti-DMPO probe in fixed tissues, cryosections were stained with Cy3-labeled streptavidin, which can bind to the biotin moiety of the albumin-Gd-DTPA-biotin contrast agent within the target tissue. Tissue sections were obtained 90 min after administration of the anti-DMPO probe. Stained tissue slices were examined with a Nikon C1 confocal laser scanning microscope (Nikon Instruments, USA).

Oxidative stress measurement

Oxidative stress was assessed by Western blotting for protein adducts to 4-hydroxynonenal (HNE) or 3-nitrotyrosine (3-NT). Mice were deeply anesthetized with isoflurane and brain tissue from the hippocampus region was collected at 6- and 24-h time points after sepsis induction and immediately frozen in dry ice. Tissue was homogenized in ice-cold Tris–HCl buffer containing protease and phosphatase inhibitor cocktails (Roche Applied Science, Indianapolis, IN, USA). Protein concentration was measured with a BCA protein assay (Thermo Scientific, Rockford, IL, USA). Protein electrophoresis was done in 4–15% gradient precast polyacrylamide gels (Bio-Rad, Hercules, CA, USA), and protein was transferred to a polyvinylidene difluoride Immobilon-FL membrane (Millipore, Billerica, MA, USA). In separate assays, mouse

monoclonal anti-HNE (Abcam, Cambridge, MA, USA) or mouse monoclonal anti-3-NT (Abcam) were incubated overnight at 1:500 dilutions in Odyssey blocking buffer. Membranes were washed three times over 5 min with PBS and incubated with secondary antibodies for 1 h at room temperature. Membranes were scanned in an Odyssey infrared imaging system (Li-Cor Biosciences, Lincoln, NE, USA).

Statistical analyses

Statistical differences between the probe-administered and the control groups were analyzed with a one-way ANOVA and a post hoc Tukey multiple-comparisons test using commercially available software (InStat; GraphPad Software, San Diego, CA, USA). A p value of less than 0.05 was considered to indicate a statistically significant difference.

Results

In vitro assessment of T_1 relaxation values for oxidatively stressed mouse astrocytes exposed to the anti-DMPO probe are shown in Fig. 2. T_1 relaxation was found to significantly decrease in vials containing mouse astrocytes exposed to H_2O_2 to form radicals that were trapped with DMPO and then tagged with the anti-DMPO probe, compared to water alone ($p < 0.0001$), astrocytes alone ($p < 0.001$), astrocytes and the anti-DMPO probe ($p < 0.0001$), astrocytes with DMPO and the anti-DMPO probe ($p < 0.0001$), or astrocytes with H_2O_2 and DMPO ($p < 0.001$), indicating the specific binding of cells with radicalized macromolecules (possibly membrane bound). Any soluble radicals trapped with DMPO or free DMPO would have been washed away from the cells and separated by centrifugation from the cell fraction before MR imaging.

Overall brain uptake of the anti-DMPO probe is depicted in Fig. 3A and B, where the mice with CLP-induced sepsis had increased uptake and overall distribution of the anti-DMPO probe throughout most regions of the brain (Fig. 3A), compared to sham mice (Fig. 3B), which seemed to restrict distribution of the anti-DMPO probe to major blood vessels, as shown by localized accumulation of the anti-DMPO probe in the highlighted areas. Detection of DMPO–nitrone adducts in various brain tissue regions (i.e., hippocampus, striatum, occipital lobe, and cortex) from septic mice (6 h post-CLP) is shown in Fig. 3C. The T_1 relaxation time was found to decrease (resulting in a significant increase in $\%T_1$ change) within all brain regions assessed in mice with CLP-induced sepsis (Fig. 3C), compared to shams. Higher significant increases in $\%T_1$ change (due to decreases in T_1 relaxation times) were found in the hippocampus, occipital, and medial cortex regions ($p < 0.001$ for all three regions), with the least significant change in $\%T_1$ within the striatum ($p < 0.01$), compared to sham controls. Fig. 4 illustrates the kinetic behavior of the anti-DMPO probe within various brain regions in septic (CLP-induced) versus sham controls. In all brain regions assessed there was a sustained significant decrease in $\%T_1$ relaxation times (all regions, $p < 0.05$) over the 75-min course studied. Relative $\%T_1$ differences were measured by comparing postcontrast (administration of the anti-DMPO probe) to precontrast image data points, where in Fig. 3 the decrease in $\%T_1$ is reported as $\%T_1$ change, and in Fig. 4 the $\%T_1$ is simply plotted.

Ex vivo detection of the anti-DMPO probe in tissue sections from mice administered the anti-DMPO probe in vivo was done by reacting Cy3-labeled streptavidin, which would target the biotin moiety of the anti-DMPO probe. CLP mice exhibited elevated fluorescence detection of the anti-DMPO probe in the hippocampus region (Fig. 5A), compared to sham animals (Fig. 5B). Elevated ex vivo DMPO adducts were also found in a CLP mouse (Fig. 5C, i and ii), compared to a sham (Fig. 5D, i and ii) by using a

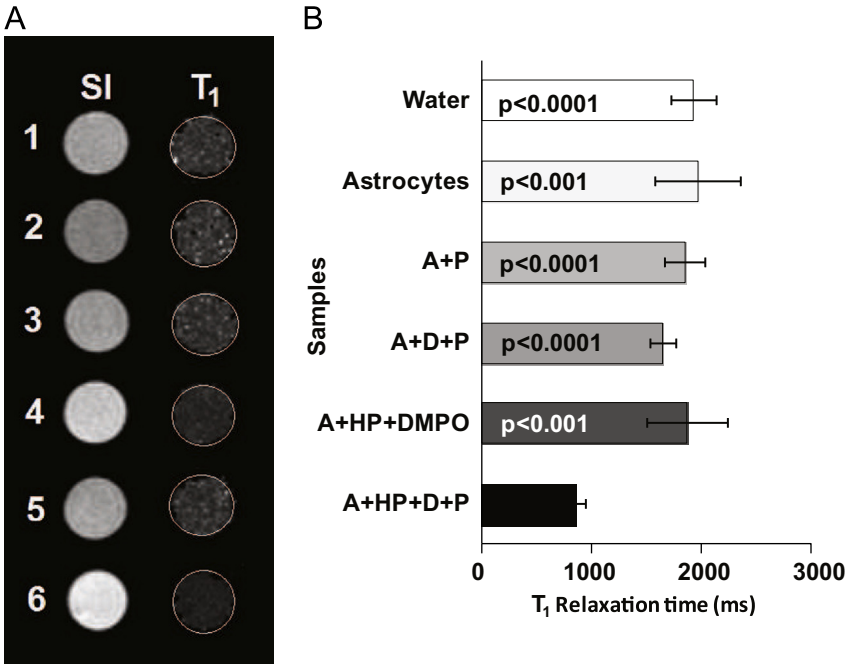

Fig. 2. In vitro assessment of the anti-DMPO probe in mouse primary astrocytes. (A) MRI signal intensities (SI; T_1-weighted) and T_1 maps (T_1) of vials containing (1) water, (2) astrocytes alone, (3) astrocytes + anti-DMPO probe (A+P), (4) astrocytes + DMPO + anti-DMPO probe (A+D+P), (5) astrocytes + H_2O_2 + DMPO (A+HP+DMPO), or (6) astrocytes + H_2O_2 + DMPO + anti-DMPO probe (A+HP+D+P). (B) T_1 relaxation values (ms) of vials containing samples 1–6 described above. Values ($n = 5$ for each group) are represented as means ± SD. There was a significant decrease in T_1 relaxation for samples containing astrocytes + H_2O_2 + DMPO + anti-DMPO probe compared to water ($p < 0.0001$), astrocytes alone ($p < 0.001$), astrocytes with anti-DMPO probe ($p < 0.0001$), astrocytes with DMPO and anti-DMPO probe ($p < 0.0001$), or astrocytes with H_2O_2 and DMPO ($p < 0.001$). T_1 relaxation was also significantly decreased for astrocytes with DMPO and anti-DMPO probe compared to water alone ($p < 0.05$).

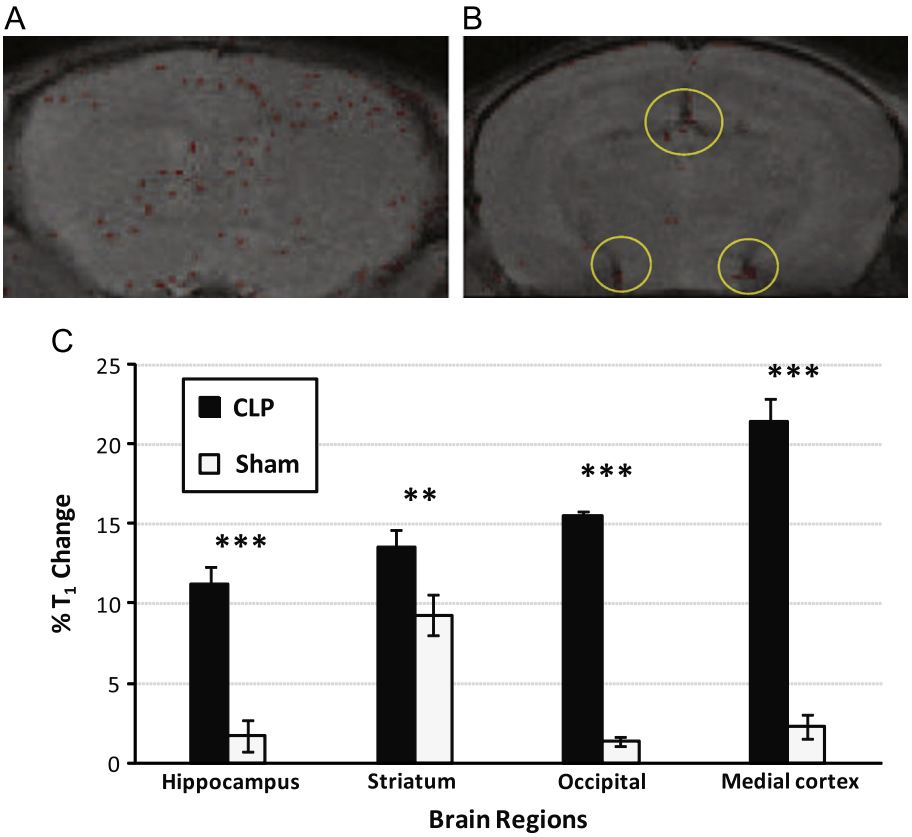

Fig. 3. In vivo molecular MR images of the anti-DMPO probe in the brains of septic and sham mice. T_1-weighted images overlaid with threshold difference images (120 min after and before administration of anti-DMPO probe) after administration of the anti-DMPO probe in the brain of (A) a mouse with CLP-induced sepsis or (B) a sham. Note the dispersed distribution of the anti-DMPO probe-associated MRI signal in the septic animal (A), compared to the restricted distribution of the anti-DMPO probe only in the blood vessels (yellow circular regions) of the sham animal. (C) Histogram of the percentage T_1 change (due to a decrease in T_1 relaxation times after compared to before contrast administration of the anti-DMPO probe) in the brains of mice with CLP-induced sepsis (CLP; $n = 3$, ROIs ≥ 10 per region) or control shams (sham; $n = 3$, ROIs ≥ 10 per region). Significantly elevated $\%T_1$ changes were found in the hippocampus ($^{***}p < 0.001$), the striatum ($^{**}p < 0.01$), the occipital lobe ($^{***}p < 0.001$), and the medial cortex ($^{***}p < 0.001$). Values are reported as means $\pm$ SD.

fluorescently labeled anti-DMPO antibody, i.e., the IST method. Elevated ex vivo anti-DMPO probe was also found in the liver (Fig. 6A vs Fig. 6B) and lungs (Fig. 6C vs Fig. 6D) of a CLP mouse compared to a sham animal.

Significantly elevated ex vivo levels of HNE, a lipid peroxidation end product, and 3-NT, an indicator of oxidized proteins, were found by Western blot in brains (hippocampus region) of septic mice compared to sham mice at 6 h post-CLP (Fig. 7A ($p < 0.05$) and B ($p < 0.05$), respectively).

Discussion

The bulk of the published studies using mMRI have relied on the specific labeling of extracellular cell surface receptors or antigens with a targeted contrast agent, although intracellular targeting is also possible. The MRI contrast agent probe is targeted to a specific receptor or antigen by an Ab or peptide. These compounds alter proton magnetization relaxation times at their sites of accumulation, making them ideal for diagnostic purposes. Paramagnetic Gd-based MR contrast agents generate a positive signal contrast (T_1 contrast), which enhances MR signal intensities of water molecules that surround these agents in T_1-weighted MR images. The T_1 contrast occurs because of a decrease in T_1 relaxation, which can be measured in T_1 maps. Gd-based probes that bind to affinity molecules have recently become popular when used with mMRI.

Our laboratory has previously used mMRI methodology to provide in vivo evidence regarding the overexpression of various tumor markers [14,21–24] in rodent glioma models. Recently we also used the same anti-DMPO probe utilized in this study to assess radical formation in a mouse diabetes model [17], in a mouse model for amyotrophic lateral sclerosis (ALS) [25], and in mouse GL261 gliomas [26]. In those studies we used a disease control, as done in this study, as well as a molecular imaging isotype control with a nonspecific IgG covalently bound to the albumin moiety of the albumin-Gd-DTPA-biotin construct instead of an anti-DMPO antibody. We did not use the IgG isotype control in this study, as we had established proof of concept in earlier studies regarding the specificity of the anti-DMPO probe for DMPO–radical adducts and that the MRI signal intensity for this IgG control was significantly lower than the signal intensity of the anti-DMPO probe in various tissues (e.g., ~42-fold in diabetic livers ($p < 0.01$) and lungs ($p < 0.05$) [17]), including the brain (e.g., ~6-fold in ALS mice ($p < 0.01$) [25] and ~3.3-fold in mouse GL261 gliomas ($p < 0.001$) [26]). Here we have used a Gd-based anti-DMPO probe with MRI detection to image free radical adducts in various regions of the brain in a mouse model for sepsis. Specifically, in a CLP-induced sepsis model we detected elevated levels of free radicals detected by an anti-DMPO probe visualized by mMRI in brain regions including the hippocampus, striatum, occipital, and medial cortex, as well as liver and lung tissues (Figs. 3–6).

IST has been used by several investigators to assess DMPO–protein adducts in various disease models. Protein radicals resulting

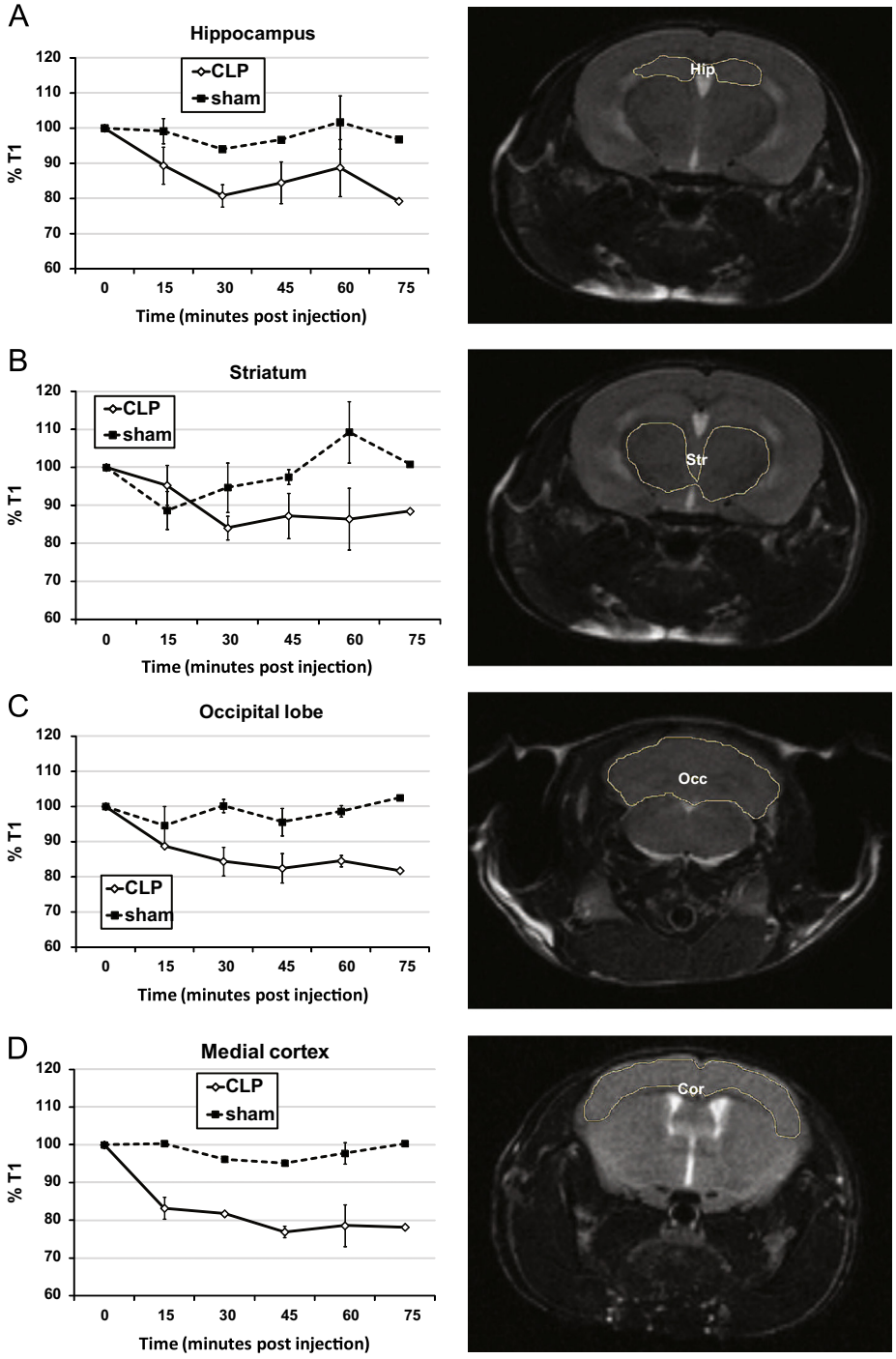

Fig. 4. Kinetic distribution of the anti-DMPO probe in septic and sham mouse brain regions. $\%T_1$ values at various time points are shown on the left, and outlined brain regions (normal mouse used for anatomical descriptions; (A) hippocampus, (B) striatum, (C) occipital lobe, and (D) medial cortex) are shown on the right. In all cases $\%T_1$ was significantly decreased ($p < 0.05$ for all regions) in septic mice (CLP-induced; $n = 3$, ROIs ≥ 10 per region) compared to sham controls ($n = 3$, ROIs ≥ 10 per region). Values are reported as means $\pm$ SD.

from the oxidation of the protein backbone or the amino acid side chains can be trapped by DMPO to form DMPO–protein adducts. These DMPO–nitrone protein adducts can then be studied by IST, which utilizes an antibody against the DMPO–nitrone adduct [9,11,12]. For instance, in vitro studies by Ramirez and colleagues [10,11] utilized IST to detect radicalized proteins in macrophages primed with endotoxin.

More generally, it is thought that the anti-DMPO probe from the in vivo targeted molecular MRI assessment conducted in this study, and our previous studies [17,25,26], primarily detects cell-associated or cell-bound DMPO–radical adducts that the anti-DMPO antibody recognizes. It is possible that the anti-DMPO probe may be internalized into the cell; however, further studies would need to be done to verify this assumption. It also should be noted that although the anti-DMPO antibody clearly has affinity for free DMPO, it was previously reported that this affinity is orders of magnitude less than that of a DMPO–protein radical adduct such as metmyoglobin–DMPO, and it was hypothesized that the covalent bond formed by the spin trapping reaction increased the recognition of the anti-DMPO antibody [9]. It is also

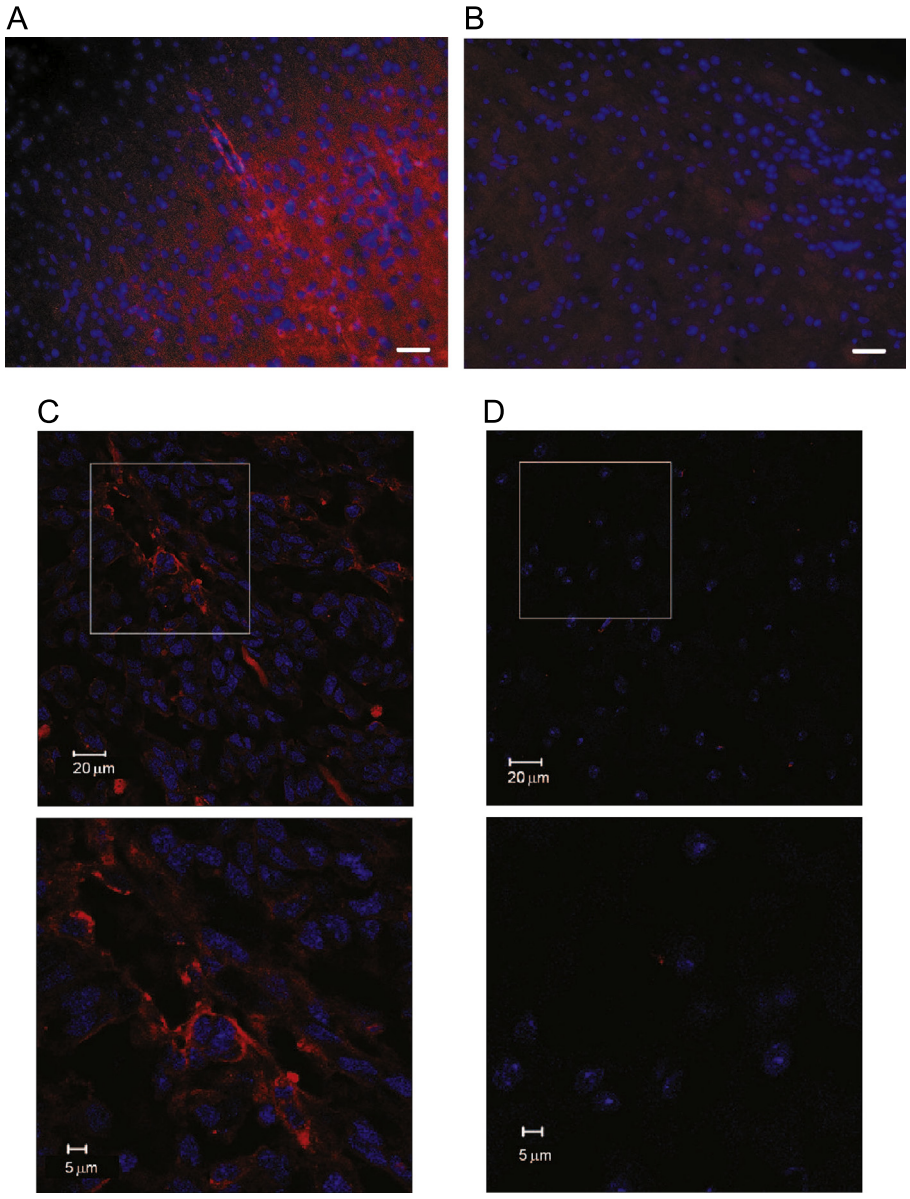

Fig. 5. Ex vivo detection of the anti-DMPO probe and DMPO–nitrone adducts in the brains of septic mice. Ex vivo fluorescence images of streptavidin–Cy3, which binds to the biotin moiety of the anti-DMPO probe in the brains of (A) mice with CLP-induced sepsis or (B) a control sham, 90 min after administration of the anti-DMPO probe. These mice were both administered DMPO and the anti-DMPO probe. Scale bars, 50 μm. Image (A) indicates that the anti-DMPO probe levels in the septic animal are higher than in the sham animal (B), because of the increase in fluorescence for the anti-DMPO probe. Nuclei are stained blue (DAPI), indicating similar cell concentrations in each sample. Ex vivo immunohistochemistry images of DMPO adducts in the brain of (Ci, ii) a mouse with sepsis and (Di, ii) a sham control. Images (C) and (D) were obtained from animals not administered the anti-DMPO probe but only DMPO to assess the level of DMPO adducts detected with immuno-spin trapping with a mouse monoclonal anti-DMPO antibody and a secondary antibody, an anti-mouse IgG–Texas red conjugate. Brain tissues were obtained 3 h after the last DMPO injection to simulate the same timing for the anti-DMPO studies. Note the increased levels of DMPO adducts in the septic animal, shown by increased fluorescence, compared to the sham animal. Cell nuclei are labeled blue (DAPI). Enlarged images shown in (ii) are taken from regions outlined in corresponding (i) images.

known that free DMPO in vivo is short-lived and is barely detected by HPLC in blood, liver, or heart tissues beyond 2 h [27]. In this study, DMPO was administered more than 2 h before the initial images were obtained after the administration of the anti-DMPO probe and more than 3 h before the last time point of the 75-min time frame for the in vivo molecular MRI assessment. The sustained $\%T_1$ decrease in the various brain regions assessed (Fig. 4) in septic animals from this study indicates that the anti-DMPO probe is binding and staying behind rather than being flushed out through the circulation. Any cell-unbound DMPO–radical adducts or free DMPO would not be detected in target tissues (such as the brain), as the body would distribute these to the blood circulation and excretory organs. In both our diabetes and our ALS studies, in which most of the mouse body was simultaneously imaged for the presence of the anti-DMPO probe, we found that anti-DMPO probe could be detected via natural distribution in the stomach, intestines, and bladder, as well as major blood vessels such as the vena cava, in addition to sustained detection in the target organs (e.g., lungs, liver, kidneys, spinal cord) studied [17,25].

Diverse molecular mechanisms of inflammation and cellular damage have been implicated in the pathogenesis of sepsis and multiple organ failure, including those related to generation of cytokines, eicosanoids, and ROS/RNS, such as nitric oxide ($^{\bullet}$NO), superoxide anions, or peroxynitrite [3]. It is well known that an underlying mechanism of sepsis involves oxidative damage due to the generation of free radicals [1–5,28–30]. Oxygen-derived free radicals generated during reperfusion after ischemia or hypoxia, or

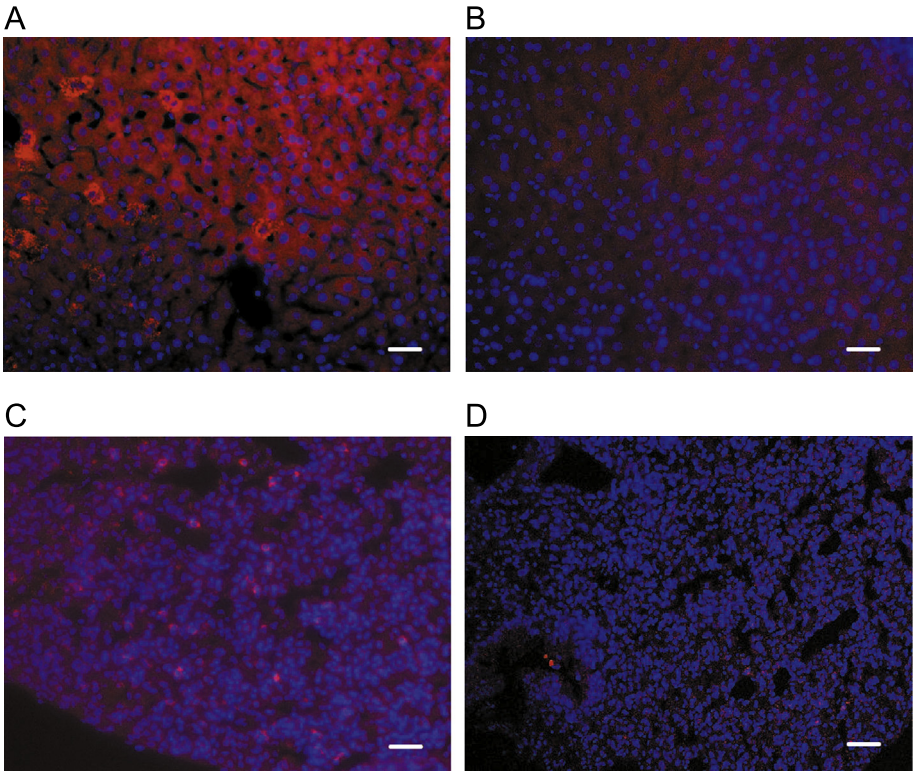

Fig. 6. Ex vivo detection of the anti-DMPO probe in the liver and lung regions of septic mice. Fluorescence images of streptavidin–Cy3, which binds to the biotin moiety of the anti-DMPO probe, in the (A) liver and (C) lung tissues of a mouse with CLP-induced sepsis, or the (B) liver and (D) lung tissues of a control sham mouse, administered DMPO and then the anti-DMPO probe. Note that elevated streptavidin–Cy3 fluorescence occurs only in tissues of the mouse with sepsis. Scale bars, 50 μm.

activated neutrophils associated with sepsis, are known to be mediators of tissue injury [3]. It is also known that lipoperoxide concentrations dramatically increase after endotoxin exposure [3]. It is thought that NF-κB plays a central role in modulating the expression of immunoregulatory mediators involved in oxidative stress and consequently in sepsis [5].

Importantly, oxidative damage is thought to be a major player in the long-lasting cognitive impairment observed in sepsis survivors [7]. Apoptosis and bioenergetic failure from ROS/RNS causing structural membrane damage and mitochondrial dysfunction, respectively, are thought to be some of the major underlying mechanisms of sepsis-associated encephalopathy and subsequent cognitive impairment [31]. Neuro-oxidative–nitrosative stress may play a major role in the molecular mechanisms underlying brain dysfunction in sepsis [31]. Sepsis is also known to induce brain mitochondrial dysfunction by causing an uncoupling of oxidative phosphorylation [32]. It is also known that alterations in cerebral microcirculation, including decreases in capillary density and leukocyte movement along the capillaries, contribute to the pathogenesis of severe sepsis [33]. In fact, a study by Gavins et al. showed that during sepsis there is a decrease in circulating leukocytes, an increase in the rolling and adhesion of leukocytes in brain microvasculature, a corresponding increase in brain myeloperoxidase activity, as well as an increase in blood–brain barrier (BBB) permeability [34]. It is also known that TNF-α increases BBB permeability, perhaps by augmenting matrix metalloproteinase-9 [35]. Sepsis is known to be associated with excessive production of TNF-α [36].

Perhaps the increased BBB permeability allows the anti-DMPO probe to target oxidized macromolecules in septic brain cells. It could be conceivable that the increased MRI signal changes are simply due to the increased amount of anti-DMPO probe in the septic brains due to the compromised BBB; however, we have previously established that an IgG-isotype contrast agent in various neurological diseases does not remain in brain [26] or spinal cord [25] tissue because of nonspecific binding, and therefore any anti-DMPO probe present in the septic mouse brain should be bound to oxidized tissue. We have also shown with ex vivo immuno-spin trapping that there is an enhanced fluorescence signal (at least 3 h after the last administration of DMPO) due to the presence of DMPO–radical adducts, which binds to the fluorescently labeled anti-DMPO antibody (Fig. 5C, i and ii). Also the presence of the anti-DMPO probe, targeted by streptavidin–Cy3 (90 min after the administration of the anti-DMPO probe) in septic mouse brains, illustrated in Fig. 5A, supports the sustained presence of the anti-DMPO probe, i.e., any unbound anti-DMPO probe would have been cleared out ~30 min postadministration (based on previous studies we conducted [25,26]).

Also of interest, Fig. 3A illustrates the diffuse distribution of the anti-DMPO probe in the brain of a septic animal, compared to a nonseptic mouse with an intact BBB, which allows the anti-DMPO probe to stay only within major blood vessels (Fig. 3B). For the septic mice, in which the BBB is compromised, it is thought the anti-DMPO probe is able to reach specific brain targets because of the presence of increased DMPO–radical adducts. It should also be noted that once the anti-DMPO probe reaches its tissue targets (e.g., brain, liver, and lungs), it is diluted from the blood (as shown with decreased probe distribution within brain blood vessels in Fig. 3A). In the sham controls, the intact BBB does not allow the anti-DMPO probe to go into brain tissue, and the lack of free radicals in these animals throughout the body results in very little binding of the anti-DMPO probe to oxidized tissues, resulting in excess anti-DMPO probe circulating in the vasculature (as seen in Fig. 3B). Previously we found in the CLP-sepsis model that there is neuronal damage and accumulation of vasogenic edema, as detected by MR spectroscopy assessment of a decrease in

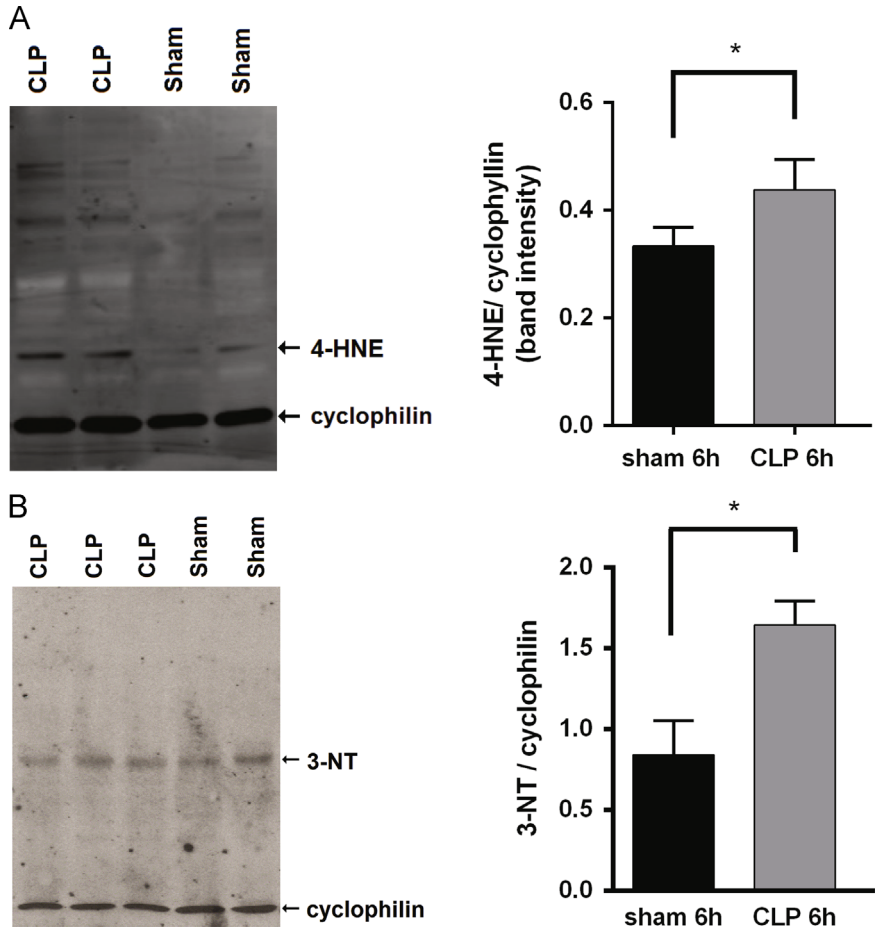

Fig. 7. Ex vivo detection of oxidized lipid and protein end products. Western blot gels (i) and Western blot quantification (ii) for (A) HNE and (B) 3-NT levels in mouse brains (hippocampus region) 6 h after CLP-induced sepsis or sham control. HNE and 3-NT band intensities were normalized to cyclophilin. Values are represented as means ± SD. Both HNE and 3-NT were significantly elevated in septic (CLP) mice ($n \geq 4$) compared to sham controls ($n \geq 4$) (*$p < 0.05$ for both).

N-acetylaspartate, a neuronal-specific metabolite, and an increased signal intensity from a T_2-weighted morphological MR image, respectively [37].

Previous studies by others have shown that the lipid peroxidation product, HNE, is elevated in the brains of baboons exposed to endotoxin, which leads to sepsis, and that the HNE generated affects the BBB and regulation of cerebral blood flow [38]. 3-NT, often associated with protein oxidation, also has been found to be elevated in brain tissue of LPS (lipopolysaccharide)-induced sepsis [39]. In our study, we have also found increased HNE and 3-NT in CLP-induced septic brains as observed by Western blot assessments of these two markers (Fig. 7). Our data, and results obtained by others, support the notion that processes associated with sepsis induce the oxidation of macromolecules such as proteins and lipids (Fig. 7). The 3-NT and HNE data also indirectly support the in vivo data regarding the binding of the anti-DMPO probe to oxidized macromolecules in septic encephalopathy, and perhaps it may be speculated that the types of DMPO-trapped macromolecular radicals that the anti-DMPO probe targets may possibly be oxidized proteins and/or lipids; however, this would have to be further studied.

It is important to note that there are varying levels of anti-DMPO-induced MRI enhancements in different brain regions of septic mice (see Fig. 3C). In a study by Semmler et al. [40], in which they induced septic encephalopathy with LPS in rats, it was established that total and neuronal cell counts decreased in the cortex and hippocampus. An earlier study by the same group determined that the hippocampus and midbrain had increased apoptosis due to sepsis [41]. If increased free radical levels correlate with increased neuronal loss, then the results of Semmler et al. may explain why we detect higher levels of the anti-DMPO probe in the hippocampus and medial cortex of septic mice compared to shams. In a study by Zhan et al. [42], in which CLP was used to induce sepsis, regional intracellular calcium in the hippocampus of septic rats was elevated compared to sham controls. It is known that elevated cytosolic calcium levels can compromise the BBB integrity [43]. We reported above that septic encephalopathy results in alterations in cerebral microcirculation, which may affect regional changes in BBB permeability. This may also explain some of the regional changes seen in the detection of the anti-DMPO probe in septic encephalopathy.

Conclusions

Here we used a combination of mMRI and IST to show for the first time noninvasive in vivo detection of radicalized macromolecules in a neurological pathology associated with sepsis. It is speculated that only radical adducts that are cell-membrane-bound (e.g., protein and/or lipid radical adducts) will be targeted by the Gd-based anti-DMPO probe and detected by MRI. Using both mMRI and IST provides the advantage of in vivo image resolution and spatial differentiation of regional events in heterogeneous tissues or organs and the regional targeting of free radical-mediated oxidation of cellular membrane components. This method can be applied toward any radical-associated pathological condition for the in vivo and in situ assessment and localization of the process of radicalization of macromolecules.

Acknowledgments

Funding was obtained by the Oklahoma Medical Research Foundation (R.A.T.) and the National Institute of Environmental Health Sciences (R.P.M.). H.C.C.F.-N. and F.A.B. were supported by CNPq, PAPES, and FAPERJ. F.A.B., M.F.O., and H.C.C.F.-N. are research scholars from CNPq and FAPERJ.

References

[1] Toklu, H. Z.; Uysal, M. K.; Kabasakal, L.; Sirvanci, S.; Ercan, F.; Kaya, M. The effects of riluzole on neurological, brain biochemical, and histological changes in early and late term of sepsis in rats. *J. Surg. Res.* **152:**238–248; 2009.

[2] Sakaguchi, S.; Iizuka, Y.; Furusawa, S.; Ishikawa, M.; Satoh, S.; Takayanagi, M. Role of Zn^{2+} in oxidative stress caused by endotoxin challenge. *Eur. J. Pharmacol.* **451:**309–316; 2002.

[3] Sakaguchi, S.; Furusawa, S. Oxidative stress and septic shock: metabolic aspects of oxygen-derived free radicals generated in the liver during endotoxemia. *FEMS Immunol. Med. Microbiol* **47:**167–177; 2006.

[4] Sakaguchi, S.; Furusawa, S.; Wu, J.; Nagata, K. Preventive effects of a biscoclaurine alkaloid, cepharanthine, on endotoxin or tumor necrosis factor-alpha-induced septic shock symptoms: involvement of cell death in L929 cells and nitric oxide production in RAW 264.7 cells. *Int. Immunopharmacol* **7:**191–197; 2007.

[5] Macdonald, J.; Galley, H. F.; Webster, N. R. Oxidative stress and gene expression in sepsis. *Br. J. Anaesth.* **90:**221–232; 2003.

[6] Neviere, R. R.; Ceepinskas, G.; Madorin, W. S.; Hoque, N.; Karmazyn, M.; Sibbald, W. J.; Kvietys, P. R. LPS pretreatment ameliorates peritonitis-induced myocardial inflammation and dysfunction: role of myocytes. *Am. J. Physiol.* **277:**H885–H892; 1999.

[7] Yokoo, H.; Chiba, S.; Tomita, K.; Takashina, M.; Sagara, H.; Yagisita, S.; Takano, Y.; Hattori, Y. Neurodegenerative evidence in mice brains with cecal ligation and puncture-induced sepsis: preventive effect of the free radical scavenger edaravone. *PLoS One* 7; 2012*e51539* 7; 2012.

[8] Federico, A.; Morgillo, F.; Tuccillo, C.; Ciardiello, F.; Loguercio, C. Chronic inflammation and oxidative stress in human carcinogenesis. *Int. J. Cancer* **121:**2381–2386; 2007.

[9] Mason, R. P. Using anti-5,5-dimethyl-1-pyrroline *N*-oxide (anti-DMPO) to detect protein radicals in time and space with immune-spin trapping. *Free Radic. Biol. Med* **36:**1214–1223; 2004.

[10] Zhai, Z.; Gomez-Mejiba, S. E.; Gimenez, M. S.; Deterding, L. J.; Tomer, K. B.; Mason, R. P.; Ashby, M. T.; Ramirez, D. C. Free radical-operated proteotoxic stress in macrophages primed with lipopolysaccharide. *Free Radic. Biol. Med.* **53:**172–181; 2012.

[11] Gomez-Mejiba, S. E.; Zhai, Z.; Della-Vedova, M. C.; Muñoz, M. D.; Chatterjee, S.; Towner, R. A.; Hensley, K.; Floyd, R. A.; Mason, R. P.; Ramirez, D. C. Immuno-spin trapping from biochemistry to medicine: advances, challenges, and pitfalls. Focus on protein-centered radicals. *Biochim. Biophys. Acta* ; 2013. (in press).

[12] Detweiler, C. D.; Deterding, L. J.; Tomer, K. B.; Chignell, C. F.; Germolec, D.; Mason, R. P. Immunological identification of the heart myoglobin radical formed by hydrogen peroxide. *Free Radic. Biol. Med.* **33:**364–369; 2002.

[13] Massot, P.; Parzy, E.; Pourtau, L.; Mellet, P.; Madelin, G.; Marque, S.; Franconi, J. M.; Thiaudiere, E. In vivo high-resolution 3D Overhauser-enhanced MRI in mice at 0.2 T. *Contrast Media Mol. Imaging* **7:**45–50; 2012.

[14] Zhelev, Z.; Aoki, I.; Gadjeva, V.; Nikolova, B.; Bakalova, R.; Saga, T. Tissue redox activity as a sensing platform for imaging of cancer based on nitroxide redox cycle. *Eur. J. Cancer* **49:**1467–1478; 2013.

[15] Dafni, H.; Landsman, L.; Schechter, B.; Kohen, F.; Neeman, M. MRI and fluorescence microscopy of the acute vascular response to VEGF165: vasodilation, hyper-permeability and lymphatic uptake, followed by rapid inactivation of the growth factor. *NMR Biomed* **15:**120–131; 2002.

[16] Towner, R. A.; Smith, N.; Tesiram, Y.; Garteiser, P.; Saunders, D.; Cranford, R.; Silasi-Mansat, R.; Herlea, O.; Ivanciu, L.; Wu, D.; Lupu, F. *In vivo* detection of c-Met expression in a rat C6 glioma model. *J. Cell. Mol. Med.* **12:**174–186; 2008.

[17] Towner, R. A.; Smith, N.; Saunders, D.; Henderson, M.; Downum, K.; Lupu, F.; Silasi-Mansat, R.; Ramirez, D. C.; Gomez-Mejiba, S. E.; Bonini, M. G.; Ehrenshaft, M.; Mason, R. P. *In vivo* imaging of immunospin-trapped radicals with molecular magnetic resonance imaging in a mouse diabetes model. *Diabetes* **61:**2401–2413; 2012.

[18] Hermanson, G. *Bioconjugate Techniques*, 456-493. New York: Academic Press; 494–527; 1996.

[19] Gomes, R. N.; Bozza, F. A.; Amâncio, R. T.; Japiassú, A. M.; Vianna, R. C.; Larangeira, A. P.; Gouvêa, J. M.; Bastos, M. S.; Zimmerman, G. A.; Stafforini, D. M.; Prescott, S. M.; Bozza, P. T.; Castro-Faria-Neto, H. C. Exogenous platelet-activating factor acetylhydrolase reduces mortality in mice with systemic inflammatory response syndrome and sepsis. *Shock* **26:**41–49; 2006.

[20] Haacke, E. M.; Brown, R. W.; Thompson, M. R.; Venkatesan, R. *Magnetic resonance imaging: physical principles and sequence design*. New York: Wiley–Liss; 367; .

[21] Towner, R. A.; Smith, N.; Asano, Y.; Doblas, S.; Saunders, D. Molecular MRI approaches used to aid in the understanding of the tissue regeneration marker Met *in vivo:* implications for tissue engineering. *Tissue Eng. Part A* **16:**365–371; 2010.

[22] Towner, R.; Smith, N.; Asano, Y.; He, T.; Doblas, S.; Saunders, D.; Silasi-Mansat, R.; Lupu, F.; Seeney, C. E. Molecular MRI approaches used to aid in the understanding of angiogenesis *in vivo:* implications for tissue engineering. *Tissue Eng. Part A* **16:**357–364; 2010.

[23] He, T.; Smith, N.; Saunders, D.; Doblas, S.; Hoyle, J.; Silasi-Mansat, R.; Lupu, F.; Lerner, M.; Brackett, D. J.; Towner, R. A. Molecular MRI assessment of vascular endothelial growth factor receptor-2 in a rat C6 glioma model. *J. Cell. Mol. Med.* **15:**837–849; 2011.

[24] Towner, R. A.; Smith, N.; Doblas, S.; Garteiser, P.; Watanabe, Y.; He, T.; Saunders, D.; Herlea, O.; Silasi-Mansat, R.; Lupu, F. In vivo detection of inducible nitric oxide synthase (iNOS) in rodent gliomas. *Free Radic. Biol. Med.* **48:**691–703; 2010.

[25] Towner, R. A.; Smith, N.; Saunders, D.; Lupu, F.; Silasi-Mansat, R.; West, M.; Ramirez, D. C.; Gomez-Mejiba, S. E.; Bonini, M. G.; Mason, R. P.; Ehrenshaft, M.; Hensley, K. In vivo detection of free radicals using molecular MRI and immuno-spin-trapping in a mouse model for amyotrophic lateral sclerosis (ALS). *Free Radic. Biol. Med.* **63:**351–360; 2013.

[26] Towner, R. A.; Smith, N.; Saunders, D.; De Souza, P. C.; Henry, L.; Lupu, F.; Silasi-Mansat, R.; Ehrenshaft, M.; Mason, R. P.; Gomez-Mejiba, S. E.; Ramirez, D. C. Combined molecular MRI and immuno-spin-trapping for in vivo detection of free radicals in orthotopic mouse GL261 gliomas. *Biochim. Biophys. Acta* ; 2013. (in press).

[27] Liu, K. J.; Jiang, J. J.; Ji, L. L.; Shi, X.; Swartz, H. M. An HPLC and EPR investigation on the stability of DMPO and DMPO spin adducts *in vivo*. *Res. Chem. Intermed* **22:**499–509; 1996.

[28] Chatterjee, S.; Lardinois, O.; Bonini, M. G.; Bhattacharjee, S.; Stadler, K.; Corbett, J.; Deterding, L. J.; Tomer, K. B.; Kadiiska, M.; Mason, R. P. Site-specific carboxypeptidase B1 tyrosine nitration and pathophysiological implications following its physical association with nitric oxide synthase-3 in experimental sepsis. *J. Immunol.* **183:**4055–4066; 2009.

[29] Chatterjee, S.; Ehrenshaft, M.; Bhattacharjee, S.; Deterding, L. J.; Bonini, M. G.; Corbett, J.; Kadiiska, M. B.; Tomer, K. B.; Mason, R. P. Immuno-spin trapping of a post-translational carboxypeptidase B1 radical formed by a dual role of xanthine oxidase and endothelial nitric oxide synthase in acute septic mice. *Free Radic. Biol. Med.* **46:**454–461; 2009.

[30] Sato, K.; Kadiiska, M. B.; Ghio, A. J.; Corbett, J.; Fann, Y. C.; Holland, S. M.; Thurman, R. G.; Mason, R. P. *In vivo* lipid-derived free radical formation by NADPH oxidase in acute lung injury induced by lipopolysaccharide: a model for ARDS. *FASEB J.* **16:**1713–1720; 2002.

[31] Berg, R. M.; Møller, K.; Bailey, D. M. Neuro-oxidative-nitrosative stress in sepsis. *J. Cereb. Blood Flow Metab.* **31:**1532–1544; 2011.

[32] D'Avila, J. C.; Santiago, A. P.; Amâncio, R. T.; Galina, A.; Oliveira, M. F.; Bozza, F. A. Sepsis induces brain mitochondrial dysfunction. *Crit. Care Med.* **36:**1925–1932; 2008.

[33] Araújo, C. V.; Estavo, V.; Tibiriçá, E.; Bozza, P. T.; Castro-Faria-Neto, H. C.; Silva, A. R. PPAR gamma activation protects the brain against microvascular dysfunction in sepsis. *Microvasc. Res.* **84:**218–221; 2012.

[34] Gavins, F. N.; Hughes, E. L.; Buss, N. A.; Holloway, P. M.; Getting, S. J.; Buckingham, J. C. Leukocyte recruitment in the brain in sepsis: involvement of the annexin 1–FPR2/ALX anti-inflammatory system. *FASEB J.* **26:**4977–4989; 2012.

[35] Tsuge, M.; Yasui, K.; Ichiyawa, T.; Saito, Y.; Nagaoka, Y.; Yashiro, M.; Yamashita, N.; Morishima, T. Increase of tumor necrosis factor-alpha in the blood induces early activation of matrix metalloproteinase-9 in the brain. *Microbiol. Immunol.* **54:**417–424; 2010.

[36] Oikonomopoulou, K.; Ricklin, D.; Ward, P. A.; Lambris, J. D. Interactions between coagulation and complement—their role in inflammation. *Semin. Immunopathol.* **34:**151–165; 2012.

[37] Bozza, F. A.; Garteiser, P.; Oliveira, M. F.; Doblas, S.; Cranford, R.; Saunders, D.; Jones, I.; Towner, R. A.; Castro-Faria-Neto, H. C. Sepsis-associated encephalopathy: a magnetic resonance imaging and spectroscopy study. *J. Cereb. Blood Flow Metab.* **30:**440–448; 2010.

[38] Zarković, N.; Zarković, K.; Schaur, R. J.; Stolc, S.; Schlag, G.; Redl, H.; Waeg, G.; Borović, S.; Loncarić, I.; Jurić, G.; Hlavka, V. 4-Hydroxynonenal as a second messenger of free radicals and growth modifying factor. *Life Sci.* **65:**1901–-1904; 1999.

[39] Ozan, G.; Turkozkan, N.; Bircan, F. S.; Balabanli, B. Effect of taurine on brain 8-hydroxydeoxyguanosine and 3-nitrotyrosine levels in endotoxemia. *Inflammation* **35:**665–670; 2012.

[40] Semmler, A.; Hermann, S.; Mormann, F.; Weberpals, M.; Paxian, S. A.; Okulla, T.; Schäfers, M.; Kummer, M. P.; Klockgether, T.; Heneka, M. T. Sepsis causes neuroinflammation and concomitant decrease of cerebral metabolism. *J. Neuroinflammation* **5:**38; 2008.

[41] Semmler, A.; Okulla, T.; Sastre, M.; Dumitrescu-Ozimek, L.; Heneka, M. T. Systemic inflammation induces apoptosis with variable vulnerability of different brain regions. *J. Chem. Neuroanat.* **30:**144–157; 2005.

[42] Zhan, R. Z.; Fujiwara, N.; Shimoji, K. Regionally different elevation of intracellular free calcium in hippocampus of septic rat brain. *Shock* **6:**293–297; 1996.

[43] Berrout, J.; Jin, M.; O'Neil, R. G. Critical role of TRPP2 and TRPC1 channels in stretch-induced injury of blood–brain barrier endothelial cells. *Brain Res* **1436:**1–12; 2012.